Free Energy Profile Decomposition Analysis for QM/MM Simulations of Enzymatic Reactions

Xiaoliang Pan,*,† Richard Van,†,‡ Jingzhi Pu,*,¶ Kwangho Nam,*,§ Yuezhi Mao,*,‖ and Yihan Shao*,†

†*Department of Chemistry and Biochemistry, University of Oklahoma, Norman, OK 73019, USA*
‡*Laboratory of Computational Biology, National, Heart, Lung and Blood Institute, National Institutes of Health, Bethesda, MD 20824, USA*
¶*Department of Chemistry and Chemical Biology, Indiana University-Purdue University Indianapolis, Indianapolis, IN 46202, USA*
§*Department of Chemistry and Biochemistry, University of Texas at Arlington, Arlington, TX 76019, USA.*
‖*Department of Chemistry and Biochemistry, San Diego State University, San Diego, CA 92182, USA*

E-mail: panxl@ou.edu; jpu@iupui.edu; kwangho.nam@uta.edu; ymao2@sdsu.edu; yihan.shao@ou.edu

Abstract

In enzyme mechanistic studies and mutant design, it is highly desirable to know the individual residue contributions to the reaction free energy barrier. In this work, we show that such free energy contributions from each residue can be readily obtained by post-processing *ab initio* quantum mechanical molecular mechanical (ai-QM/MM) free energy simulation trajectories. Specifically, through a mean force integration along the minimum free energy pathway, one can obtain the electrostatic, polarization, and van der Waals contributions from each residue to the free energy barrier. Separately, a similar analysis procedure allows us to assess the contribution from different collective variables along the reaction coordinate. The chorismate mutase reaction is used to demonstrate the utilization of these two trajectory analysis tools.

1 Introduction

Enzymes acquire their catalytic power by lowering the reaction free energy barrier either through stabilizing the transition state or destabilizing the reactant.[1–3] Accordingly, the natural and laboratory-directed evolutions of enzymes capitalize on the mutation of enzyme residues to further lower the free energy barrier and thereby increase the enzyme activity. In enzyme mechanism studies and design, it is clearly desirable to assess various components of free energy changes.[4–7] Over the years, many schemes have been developed to quantify the detailed contribution from individual residues to the enzyme reaction energy barriers.[8–15] In general, these schemes fall into several categories:

Successive residue charge deletion. A first-order perturbation estimate for the residue (electrostatic) contributions to the energy along a reaction pathway was developed in the early 1990s by Karplus and coworkers.[8] In particular, residue molecular mechanical (MM) charges were successively set to zero starting from those furthermost from the active site to the closest ones, while monitoring the energy change within a combined quantum mechanical molecular mechanical (QM/MM) description of the enzyme system. This analysis technique was employed by Karplus and coworkers to identify key residues of the triosephosphate isomerase[8–10] and by Gao and coworkers to interpret the role of various dihydrofolate reductase residues on its catalysis.[11]

Single residue charge deletion. It was first proposed by Mulholland and coworkers in the early 2000s to explore the effects of individual residues along a QM/MM minimum energy pathway (MEP) of chorismate mutase reaction.[12] Within the approach, the charges of a *single residue* of interest was deleted from a MEP structure, while leaving all other residues intact, yielding the residue contribution to the QM/MM electrostatic energy. Relatedly, Jaña and coworkers assessed the stabilization effects of the lysine and arginine residues in different conformations of acetohydroxyacid synthase by turning off the partial charges on these residues.[16] They also estimated the polarization effects of an arginine residue by calculating the change in the natural bond orbital charges on the carbonyl group of the ligand after switching off the partial charges on the arginine residue.

Energy decomposition analysis. It is, in its spirit, related to the single residue charge deletion methods above and to the linear response approximation (LRA) method from Warshel and coworkers[17,18] and the electrostatic free energy response (EFER) method from Florian and coworkers.[19] In this particular analysis, Cisneros and coworkers averaged the electrostatic contribution from the *i*-th residue to the QM/MM interaction energy at both the transition state and the reactant. The residue contribution difference was examined in the study of DNA polymerase I, glutamine-dependent amidotransferase, CRISPR-Cas9 catalyzed DNA target strand cleavage, and many other enzyme systems.[20–23]

Catalytic field analysis. Szefczyk *et al.* defined the static catalytic field as the difference of the QM/MM electrostatic potentials of the reactant and transition states.[13,24] A map of the static catalytic field onto an isodensity surface around the substrate was shown to be helpful for understanding whether each charged residue (near the isodensity surface) increases or decreases the activation barrier.

Local electrostatic potential analysis. The local electrostatic environment, which includes the local electrostatic potential and the local electric field, of the active site has been studied for decades,[3,25–30] underlying the general notion that electrostatic preorganization by the enzyme reduces the free energy barrier and provides the enzyme catalytic power.[1] The electrostatic potential on key active site atoms has been explored by Moliner and coworkers to explain the effect of enzyme conformations on the catalytic rate constants of Kemp eliminase,[31] to test the hypotheses for the catalytic mechanism of glycine N-Methyltransferase,[32] and to enhance the secondary amidase activity of *Candida antarctica* lipase B variants (by adopting electrostatically more favorable residues from *Bacillus subtilis* esterase Bs2).[33]

Local electric field analysis. The local electric field in the active site has been studied for many enzymes, such as ketosteroid isomerase,[34–37] liver alcohol dehydrogenase,[38,39] dihydrofolate reductase,[40] Kemp eliminase,[14,15] cytochrome P450,[41] heme-iron

oxidoreductase,[42] acid phosphatases,[43] tyrosine hydroxylase,[44] and uracil-DNA glycosylase.[45] Experimentally, the local electric field, such as that on the C=O bond of ketosteroid isomerase,[34–36,38] can be measured using calibrated vibrational Stark probes. Computationally, the local electric field on a key chemical bond in the active site can be readily evaluated using a fixed-charge or polarizable MM[14,15] description of the enzyme environment, by taking the mean of the field values at the atomic sites[14,46] or calculating the field at the bond midpoint or critical point.[37] A decomposition of the local electric field change from the reactant to the transition also leads to individual residue contributions to the reaction energy barrier, which is key to the understanding of enzyme activities and the development of potent enzyme variants. Relatedly, the local electrostatic force along breaking bonds (*i.e.* difference between the product of local electric potential and atomic charges on the endpoints) provided insight into the catalytic mechanism of HIV-1 Protease[47] and *Candida antarctica* lipase B.[48]

Inspired by and building upon all these efforts, here we introduce two new trajectory analysis tools for *ab initio* QM/MM free energy simulations of enzyme reactions. Using these tools, the QM/MM free energy profile of the simulated system (such as a wild-type enzyme) can be readily decomposed into contributions from individual residues or from key reaction coordinates. We expect these tools to be helpful to enhance our mechanistic understandings of enzyme functions and facilitate the development of enzyme variants.

Compared to the analysis techniques mentioned above, our new tools differ in a number of ways. First, they provide the free energy contributions (instead of enthalpic ones) from each residue or reaction coordinate. Second, we account for not only electrostatic contributions from each residue, but also polarization and vdW effects. Third, unlike the first-order perturbation estimate, our analysis results do not depend on the particular order of the residues considered. Lastly, a heat map will also be generated from our analysis, but it is a 3-d map instead of a surface map (like the 2-d catalytic field map).

2 Theory

2.A Free Energy Profile by Mean Force Integration

Free energy profile, which is defined as the free energy change along a reaction coordinate ξ, can be expressed as

$$A(\xi) = -\frac{1}{\beta}\ln P(\xi) + A_0, \tag{1}$$

where $P(\xi)$ is the probability density to find the system at ξ and A_0 is a constant. For a particular value of ξ, one can regard $A(\xi)$ as the free energy of the state corresponding to an iso-ξ hypersurface in the phase space.

To efficiently compute the free energy profile, one often resorts to umbrella sampling.[49] Here, the one-dimensional reaction coordinate ξ is divided into a series of windows, and a biasing potential

$$V_i^b(\xi) = \frac{1}{2}k_i(\xi - \xi_i)^2 \tag{2}$$

is added to the unbiased system energy, E^u, for the window i, i.e.,

$$E_i^b = E^u + V_i^b(\xi). \tag{3}$$

Similar to the umbrella integration,[50] the free energy profile is calculated by integrating the unbiased free energy gradient over the reaction coordinate ξ,

$$A^u(\xi') = \int_{\xi_0}^{\xi'} \frac{\partial A^u(\xi)}{\partial \xi}\mathrm{d}\xi + C. \tag{4}$$

In practice, it can be computed discretely as

$$A_i^u = \sum_{m=0}^{i-1} \frac{1}{2}\left(\frac{\partial A_m^u}{\partial \xi} + \frac{\partial A_{m+1}^u}{\partial \xi}\right)(\xi_{m+1} - \xi_m), \tag{5}$$

where the free energy gradient along the pathway is

$$\frac{\partial A_m^u}{\partial \xi} = \left\langle \frac{\partial E^u}{\partial \xi} \right\rangle_{\xi=\xi_m}^b, \tag{6}$$

and the energy gradient for each configuration is[51–54]

$$\frac{\partial E^u}{\partial \xi} = \frac{\partial E^u}{\partial \mathbf{x}} \cdot \frac{\partial \mathbf{x}}{\partial \xi} + \beta^{-1}\frac{\partial \ln|J|}{\partial \xi}, \tag{7}$$

where $\mathbf{x}$ represents the Cartesian coordinates involved in ξ and J is the Jacobian. By using Eqs. 6 and 7, we can decompose the total energy into different energy terms and calculate the free energy profile contributions from each of them.

2.B Decomposition by QM/MM Energy Term

In QM/MM calculations, the system is divided into a quantum mechanical (QM) subsystem and a MM subsystem. The total potential energy of the system can be expressed as

$$E = E_{\mathrm{QM}} + E_{\mathrm{QM-MM}} + E_{\mathrm{MM}}, \tag{8}$$

where E_{QM} is the potential energy of the isolated QM subsystem, $E_{\mathrm{QM-MM}}$ is the interaction energy between the QM and MM subsystems, and E_{MM} is the potential energy within the MM subsystem.

For simplicity, here we shall focus on cases where there are no covalent bonds linking the QM and MM regions. For those cases, the interaction energy, $E_{\mathrm{QM-MM}}$, is the sum of contributions from the electrostatic and van der Waals (vdW) interactions,

$$E_{\mathrm{QM-MM}} = E_{\mathrm{QM-MM}}^{\mathrm{elec}} + E_{\mathrm{QM-MM}}^{\mathrm{vdW}}. \tag{9}$$

The QM-MM electrostatic interaction can be further divided into permanent electrostatics and polarization terms,[4]

$$E_{\mathrm{QM-MM}}^{\mathrm{elec}} = E_{\mathrm{QM-MM}}^{\mathrm{perm}} + E_{\mathrm{QM-MM}}^{\mathrm{pol}}, \tag{10}$$

where the permanent electrostatics term, $E_{\mathrm{QM-MM}}^{\mathrm{perm}}$, is the interaction energy between the "unpolarized" QM subsystem (its wave function remains at the reference state, e.g., gas-phase) and the MM subsystem. The polarization term, $E_{\mathrm{QM-MM}}^{\mathrm{pol}}$, accounts for the energy change of "relaxing" the QM wave function to accommodate the MM environment.

2.C Decomposition of QM/MM Interaction Energies by Residue

It should be noted that decomposing potential of mean force (PMF) by the mean force contributions has been done previously by several groups to analyze the MM simulations.[55,56] Following those work, here we shall try to decompose PMF in the context of QM/MM simulations.

As stated in the introduction, our goal is to estimate the contributions from difference parts of the MM subsystems to the chemical transformation in the QM subsystem. This can be achieved by decomposing the total QM-MM interaction energy into terms that interact the QM subsystem with *each MM atom* and then grouping them together by residue or protein domain.

For the QM-MM electrostatic interaction, the permanent electro-

statics term can be easily decomposed as

$$E^{\text{perm}}_{\text{QM-MM}} = \sum_B \phi^0_B q_B, \tag{11}$$

where ϕ^0_B is the electrostatic potential on the MM atomic site B from the "unpolarized" QM subsystem, and q_B is the partial charge of the MM atom B. To obtain the corresponding nuclear gradients in Eq. 7 for each configuration, the derivatives of the QM electrostatic potential, $\frac{\partial \phi^0_B}{\partial \mathbf{x}}$, need to be computed either via finite difference (by displacing those QM atoms that are involved in the reaction coordinate ξ) or analytically (by solving the coupled-perturbed Kohn-Sham equations for QM orbital responses). The finite-difference approach is adopted in our implementation.

Strictly speaking, the polarization term cannot be decomposed into contributions by the MM atoms since they are not additive. However, the polarization term can be written as[4]

$$E^{\text{pol}}_{\text{QM-MM}} = E^{\text{dist}}_{\text{QM-MM}} + \Delta E_{\text{QM-MM}}, \tag{12}$$

where both $E^{\text{dist}}_{\text{QM-MM}}$ and $\Delta E_{\text{QM-MM}}$ are both due to the polarization/distortion of the QM wavefunction. But $E^{\text{dist}}_{\text{QM-MM}}$, the electron distortion energy, is the net increase in E_{QM}, whereas $\Delta E_{\text{QM-MM}}$ is the net decrease in $E^{\text{elec}}_{\text{QM-MM}}$. The classical linear response theory[4,57,58] implies that, to first order, $E^{\text{dist}}_{\text{QM-MM}}$ is equal to $-\frac{1}{2}\Delta E_{\text{QM-MM}}$. Thus in this work, the QM/MM polarization energy is approximately decomposed as

$$\tilde{E}^{\text{pol}}_{\text{QM-MM}} = \frac{1}{2}\Delta E_{\text{QM-MM}} = \frac{1}{2}\sum_B (\phi_B - \phi^0_B) q_B, \tag{13}$$

where ϕ_B is the electrostatic potential on the MM atomic site B from the polarized QM subsystem. To obtain the the nuclear gradient of the QM-MM polarization energy, the finite-difference approach was also used to compute $\frac{\partial \phi_B}{\partial \mathbf{x}}$.

In Eq. 9, the QM-MM vdW interaction is rather straightforward to decompose by MM atoms, since it is typically calculated as a pair-wise additive potential at the MM level, i.e.,

$$E^{\text{vdW}}_{\text{QM-MM}} = \sum_{B\in\text{MM}} \sum_{A\in\text{QM}} 4\varepsilon_{A,B}\left[\left(\frac{\sigma_{A,B}}{r_{A,B}}\right)^{12} - \left(\frac{\sigma_{A,B}}{r_{A,B}}\right)^{6}\right]. \tag{14}$$

The nuclear gradient of this energy, which is purely classical, is rather straightforward to evaluate.

2.D Decomposition by Collective Variables

Let us consider the case where the reaction coordinate is a linear combination of K collective variables (CVs),

$$\xi = \sum_{k=0}^{K-1} c_k z_k. \tag{15}$$

Following the umbrella sampling simulation,[49] one can compute the average collective variables, $z_{k,m}$, for the m-th sampling window. The corresponding gradient with respect to the reaction coordinate can be obtained either through finite-difference,

$$\frac{\partial z_{k,m}}{\partial \xi} = \frac{z_{k,m+1} - z_{k,m}}{\xi_{m+1} - \xi_m}, \tag{16}$$

or analytically through fitting each z_k with cubic spline, namely $z_k = z_k(\xi)$. From Eq. 15, it is clear that

$$\sum_{k=0}^{K-1} c_k \frac{\partial z_{k,m}}{\partial \xi} = 1, \tag{17}$$

which applies to each window. This provides a convenient way to decompose the free energy gradient with respect to the reaction coordinate into contributions from each CV

$$\frac{\partial A^u_m}{\partial \xi} = \sum_{k=0}^{K-1} c_k \frac{\partial A^u_m}{\partial \xi}\frac{\partial z_{k,m}}{\partial \xi}, \tag{18}$$

where the integration of $c_k \frac{\partial A^u_m}{\partial \xi}\frac{\partial z_{k,m}}{\partial \xi}$ along the pathway captures the effect of each CV on the free energy profile.

3 Computational Details

The trajectories for the analysis were taken from our previous study,[59] where a detailed simulation protocol can be found. In brief, the initial structure was built upon the X-ray crystal structure (PDB ID: 2CHT[60]) of *Bacillus subtilis* chorismate mutase complexed with a transition state analog, which was modified to the substrate chorismate manually. The resulting structure was solvated in a cubic box of TIP3P[61] water molecules, and sodium counterions were added to neutralize the system. The system was first equilibrated at 300 K and 1 atm using Langevin dynamics with a friction coefficient of 5 ps^{-1} and Berendsen barostat with a relaxation time of 1 ps under the periodic boundary conditions, where the substrate and the enzyme were modeled using GAFF[62] and the AMBER ff14SB force field,[63] respectively.

After the equilibration, QM/MM umbrella sampling[49] simulations were conducted at 300 K and constant volume to simulate the bond breaking/forming process. The substrate was described by density functional theory (DFT) with the B3LYP functional[64–66] and 6-31G* basis set,[67] while the rest of the system (protein and solvent) was described by the force fields used in the classical simulations. For both the classical and QM/MM simulations, the particle mesh Ewald (PME) method[68,69] was used to treat the MM-MM electrostatic interactions, while the van der Waals interactions were truncated at the cutoff of 10 Å. The QM/MM-AC method[70] was used to capture the long-range QM-MM electrostatic interactions. The SHAKE algorithm[71] was used to constrain all bonds involving hydrogen atoms except for those in the QM region during the QM/MM simulations, and time steps of 2 fs and 1 fs were used for MD integration using the leapfrog integrator for the classical and QM/MM simulations, respectively. The classical MD simulations were performed using the PMEMD program from the Amber20 package.[72] The QM/MM MD simulations were performed using our QM/MM interface QMHub (https://github.com/panxl/qmhub) and a modified version of the SANDER program from the AmberTools20 package.[72] All DFT/MM energy/force calculations were performed using Q-Chem 5.2.[73]

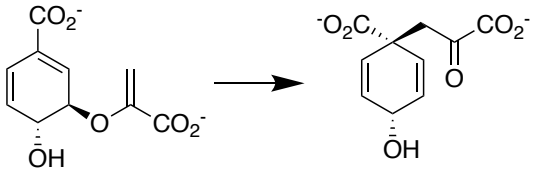

Figure 1: Scheme for the chorismate mutase reaction.

For umbrella sampling simulations of the chorismate mutase reaction (Fig. 1), the reaction coordinates were defined as $\xi = d_{C\text{–}O} - d_{C\text{–}C}$, where $d_{C\text{–}O}$ and $d_{C\text{–}C}$ were the bond lengths of the breaking and forming bonds, respectively. A total of 80 windows were evenly distributed with an interval of 0.05 Å to cover ξ ranged from -1.975 to 1.975 Å, and the force constants were set to be 150 kcal/mol/Å^2 for all the windows. The Hamiltonian replica exchange molecular dynamics (HREMD)[74] technique was used to accelerate the convergence of the free energy simulations, in which the exchanges of the biasing potentials between the neighboring windows were attempted every 100 steps. For each window, 50 ps simulation was conducted, and the configurations were saved every 0.1 ps, which resulted in 500 configurations. The `pymbar` package (https://github.com/choderalab/pymbar) was used for the calculation of the free energy profile using the multistate Bennett acceptance ratio (MBAR)[75] method.

4 Results and Discussion

4.A Validation of the Mean Force Integration

For our analysis of chorismate mutase reaction free energy, the trajectories were generated in our previous study[59] and included 80 windows of replica–exchange umbrella sampling simulations.[76] Each of the trajectories was 50 ps in length, where 300 configurations from the last 30 ps were used to calculate the mean forces along the reaction coordinate. The trapezoidal rule (Eq. 5) was used in thermodynamic integration (TI) to estimate the free energy profile and its uncertainties. We also calculated the free energy profile using the MBAR method for comparison. These two analyses produced nearly the same free energy profiles within statistical uncertainty (Fig. 2), and the free energy barriers and reaction free energies calculated from the two methods were almost identical (Table 1), even though larger uncertainties were associated with the TI analysis.

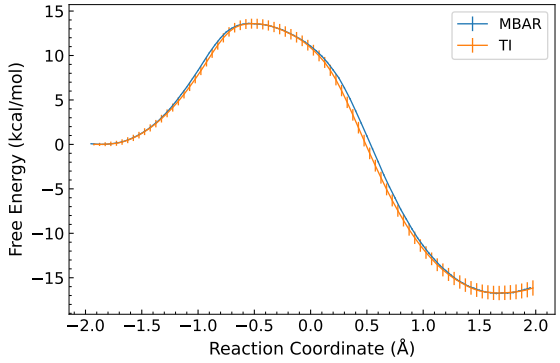

Figure 2: Comparison of the free energy profiles of the chorismate mutase reaction calculated from MBAR and TI.

It should be noted that, strictly speaking, only the result from MBAR was the free energy profile, while TI yielded the potential of mean force. The difference between them was the Jacobian term (also shown in Table 1) that originated from the use of non-Cartesian reaction coordinates. In the context of enzymatic reactions, distance-based reaction coordinates are often adopted. In this case, the Jacobian term accounted for the fact that a larger distance for the reaction coordinate corresponded to a larger volume in the phase space. However, in practice, the increased phase space at larger distances was hardly ever sampled during umbrella sampling simulations of enzymatic reactions, since the presence of the enzyme hindered the sampling of the rotational degrees of freedom. Since the Jacobian term is often small (see Table 1) and does not directly depend on the potential energy of the system, we did not include its contribution in our subsequent analyses.

Table 1: Free Energy Barriers ($\Delta A^{\ddagger}$) and Reaction Free Energies (ΔA) for the Chorismate Mutase Reaction using MBAR and TI

	Free Energy Barrier (kcal/mol)	Reaction Free Energy (kcal/mol)
MBAR	13.6 ± 0.1	-16.8 ± 0.1
TI	13.6 ± 0.6	-16.7 ± 0.8
Jacobian[a]	0.2 ± 0.0	0.0 ± 0.0

[a] The Jacobian contributions were not included in the TI results. The standard deviations are ∼0.001 kcal/mol.

4.B Decomposition by the QM/MM Energy Components

The TI-integrated QM/MM free energy profile (orange curve in Fig. 2 and purple curve in Fig. 3) was divided into contributions from QM/MM energy terms, namely, gas-phase, permanent electrostatic, polarization, and QM/MM vdW energies according to Eqs. 8, 9, and 10, with the results shown in Fig. 3. The corresponding free energy barrier and reaction free energy components were collected in Table 2. As expected, the gas-phase free energy barrier was much higher (20.3 - 13.6 = 6.7 kcal/mol) than the QM/MM free energy barrier. In other words, the free energy barrier was reduced by 6.7 kcal/mol because of the substrate-enzyme (QM-MM) interactions.

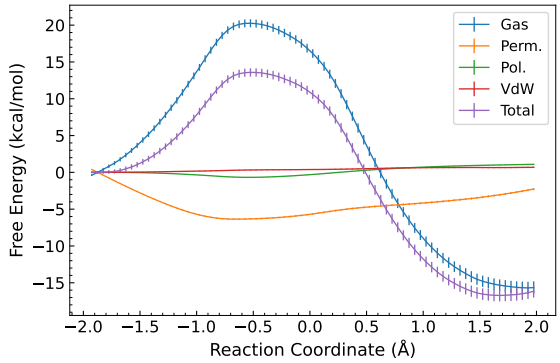

Figure 3: Decomposition of the free energy profile of the chorismate mutase reaction by the QM/MM energy components.

As shown in Table 2, such a lowering of the barrier height arose mainly from the QM-MM electrostatics, which was around -7.0 kcal/mol. In contrast, the QM-MM van der Waals raised the barrier by 0.3 kcal/mol. A further analysis of the QM-MM electrostatic interactions suggested that 90% of the corresponding free energy change (~ -6.3 kcal/mol) was caused by the QM/MM permanent electrostatics, with the remaining 10% (~ -0.7 kcal/mol) coming from the polarization/distortion of the QM wavefunction.

For the reaction free energy, the difference between gas-phase and QM/MM values was much smaller. The reduction due to the QM-MM permanent+polarizaton electrostatics changed from -7.0 kcal/mol (barrier) to -2.0 kcal/mol (reaction). It was further offset by a slightly larger free energy increase due to the QM-MM vdW interactions from 0.3 kcal/mol (barrier) to 0.7 kcal/mol (reaction). Overall, the QM/MM reaction free energy was only -16.7 - (-15.3) = -1.4 kcal/mol lower than the gas-phase value, which suggests that

Table 2: Decomposition of the Free Energy Barriers and Reaction Free Energies for the Chorismate Mutase Reaction by QM/MM Energy Components

	Free Energy Barrier (kcal/mol)	Reaction Free Energy (kcal/mol)
Gas	20.3 ± 0.5	-15.3 ± 0.8
Perm.	-6.3 ± 0.1	-3.0 ± 0.1
Pol.	-0.7 ± 0.0	1.0 ± 0.0
VdW	0.3 ± 0.1	0.7 ± 0.1
Total	13.6 ± 0.6	-16.7 ± 0.8

the binding free energy difference between the reactant and product was relatively small.

It should be noted that in our work the QM-MM vdW interaction was calculated at the MM level, and the same set of Lennard-Jones parameters were used throughout the entire reaction. So the contribution from the QM-MM vdW interactions might not be optimally estimated, especially towards the product side since the parameters were modeled based on the atom types of the reactant. Density-dependent QM/MM vdW interactions [77–80] will be explored in our future work.

4.C Decomposition of the QM/MM Interactions by Residues

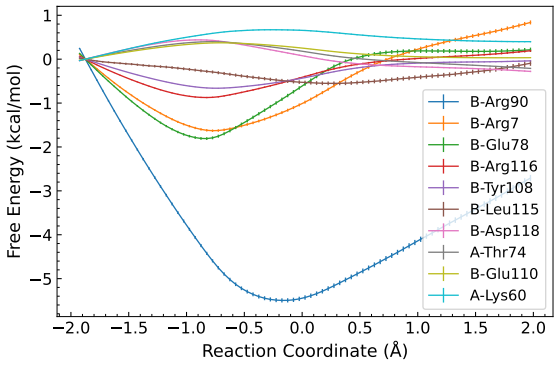

Figure 4: The free energy profile contributions from selected residues of chorismate mutase.

The free energy profile contributions from the total QM/MM interaction energy and its components were further decomposed by the interaction between the QM region and each of the MM atoms according to Eqs. 11 and 13. The atomic contributions from the enzyme were then grouped together by residues, while the ones from the solvent and counterions were grouped together by their distances to the QM region into near- and far-field solvent contributions. The residues that changed the free energy barrier by at least 0.3 kcal/mol were listed in Table 3, and the free energy profile contributions for some of these residues were presented in Fig. 4. The residues that have the most influence on the barrier are several charged residues near the substrate, namely, Arg90, Arg7, Glu78, and Arg116 and a polar residue Tyr108, which are consistent with the mutagenesis studies. [81,82] While most of the effects from the residues are dominated by the permanent electrostatics which are followed by polarization effect, the non-polar residue Leu115 reduce the barrier by 0.4 kcal mol through the vdW interaction (Table 3).

Overall, our results are consistent with previous computational studies, where Arg90 and Arg7 have been highlighted as important residues for the enzyme activity. [12,13,83–87] We note that less consistent results have been reported for the effects of Glu78 [12,13,83–87] and Tyr108. [13,84,85] The catalytic importance of Leu115 has also been reported. [87]

Since most of the studies that analyze the residue contributions to the barrier changes used the difference of interaction energies between the residues in the MM subsystem and the QM subsystem for the reactant and transition state configurations, instead of integrating the mean forces of the interaction energies along the reaction coordinate as in this work, we wanted to compare the two approaches. We used Eqs. 11, 13, and 14 to calculate the different components of the interaction energies between the residues in the MM subsystem (the protein and solvent) and the QM subsystem (the substrate) (Table S1). In general, the residues that showed the largest contributions from these energy-based calculations are consistent with the mean force based analysis (Table 3), namely, Arg90, Arg7, Glu78, Arg116, and Lys60. But the energy-based analysis showed much larger absolute contributions to the barrier and uncertainties, which makes the mean force-based analysis more reliable.

To visualize the effects of the residues in the enzyme in the 3D space, we defined a free energy barrier potential for each atom in the enzyme as the free energy barrier contribution from the particular atom divided by its partial charge, i.e., for the atom i in the enzyme, its free energy barrier potential $\phi_i^{\ddagger}$ can be calculated as

$$\phi_i^{\ddagger} = \frac{\Delta\Delta G_i^{\ddagger}}{q_i}, \tag{19}$$

where $\Delta\Delta G_i^{\ddagger}$ is the free energy barrier contribution from the atom i and q_i its partial charge. Then we can visualize the free energy barrier potentials by mapping them onto the atoms of the enzyme in its crystal structure (Fig. 5). Such a free energy barrier potential provides a 3D "heatmap" for suggesting mutations to modulate the activity of the enzyme.

4.D Decomposition by Collective Variable

The total free energy profile was also divided into contributions from individual collective variables according to Eq. 18. As shown in Fig. 6, the reaction falls into four stages. In stage I of the reaction (with the reaction coordinate within -2.0 Å to -0.9 Å), the progressing of the reaction coordinate mainly arose from the reducing of the C–C distance (Fig. 6A). Correspondingly, the free energy increase mainly came from the d_{C-C} component (Fig. 6B). This is reversed in stage II (-0.9 Å to -0.5 Å), where the C–O bond broke while the C–C distance changed only marginally. During that stage, it was the C–O bond breaking that caused a further free energy increase. By the end of stage II, the reaction reached the transition state.

As the reaction continued in stage III (-0.5 Å to 0.5 Å), the free energy of the system started to decrease, which was mainly due to the formation of the C–C bond. In stage IV (0.5 Å to 2.0 Å), the d_{C-O} distance continued to increase, which further decreased the free energy of the system to a plateau for the product by the end of stage IV.

4.E Decomposition by Residue and Collective Variables

The free energy contributions from individual residues in Section 4.C can be further decomposed by collective variables, leading to Fig. 7. It was clear that, out of the key residues, Arg90 reduced the free energy barrier through both C–O and C–C distances during stage I,

Table 3: Decomposition of Free Energy Barrier Change for the Chorismate Mutase Reaction by Residues.

Residue	Perm. (kcal/mol)	Pol. (kcal/mol)	VdW (kcal/mol)	Total (kcal/mol)
B-Arg90	-5.60 ± 0.01	-0.47 ± 0.00	0.84 ± 0.04	-5.22 ± 0.04
B-Arg7	-1.42 ± 0.01	-0.11 ± 0.00	-0.00 ± 0.00	-1.52 ± 0.03
B-Glu78	-0.93 ± 0.01	-0.54 ± 0.00	-0.01 ± 0.00	-1.48 ± 0.04
B-Arg116	-0.64 ± 0.00	-0.14 ± 0.00	0.02 ± 0.00	-0.76 ± 0.02
B-Tyr108	-0.57 ± 0.00	-0.08 ± 0.00	0.01 ± 0.00	-0.63 ± 0.01
B-Leu115	-0.03 ± 0.00	0.05 ± 0.00	-0.40 ± 0.03	-0.38 ± 0.04
B-Lys111	-0.26 ± 0.00	-0.06 ± 0.00	0.00 ± 0.00	-0.32 ± 0.00
A-Glu78	-0.21 ± 0.00	-0.09 ± 0.00	0.00 ± 0.00	-0.30 ± 0.00
B-Asp118	0.24 ± 0.00	0.09 ± 0.00	0.00 ± 0.00	0.33 ± 0.01
A-Thr74	0.24 ± 0.00	0.12 ± 0.00	-0.00 ± 0.00	0.36 ± 0.01
B-Glu110	0.29 ± 0.00	0.07 ± 0.00	0.00 ± 0.00	0.36 ± 0.00
A-Lys60	0.58 ± 0.00	0.06 ± 0.00	0.01 ± 0.00	0.65 ± 0.01
Near Solvents[a]	0.84 ± 0.08	-0.04 ± 0.01	-0.01 ± 0.01	0.84 ± 0.08

[a] Solvent molecules and counter-ions that are within 10 Å of the QM region.

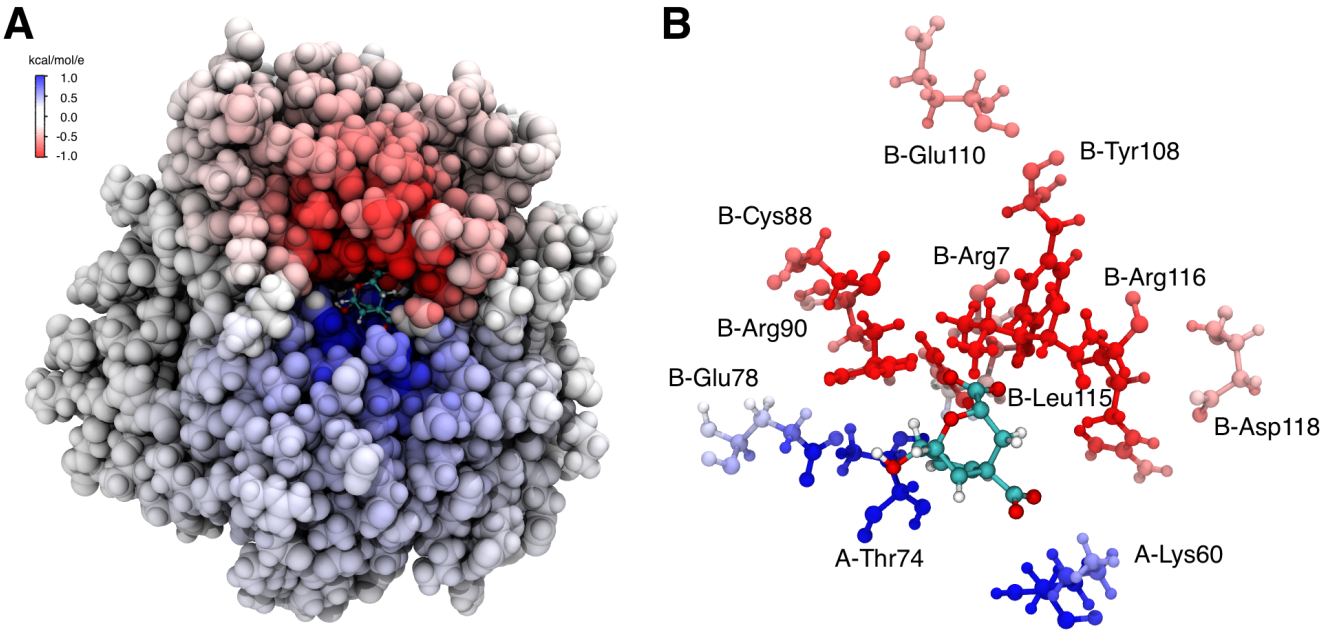

Figure 5: A) Free energy barrier potentials mapped onto the crystal structure of chorismate mutase, B) and the close-up version with only the selected residues shown.

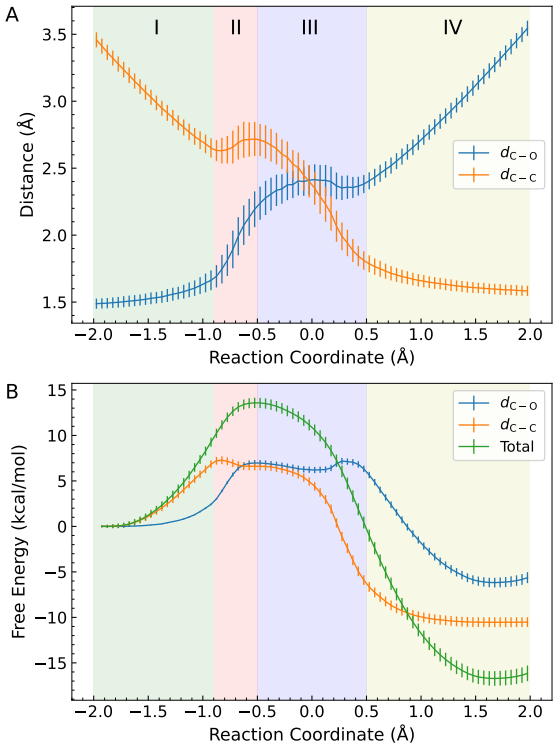

Figure 6: (A) Changes of the individual collective variables (d_{C-O} and d_{C-C}) with respect to the reaction coordinate ($d_{C-O} - d_{C-C}$) in the sampled pathway. (B) Decomposition of the free energy profile by collective variable.

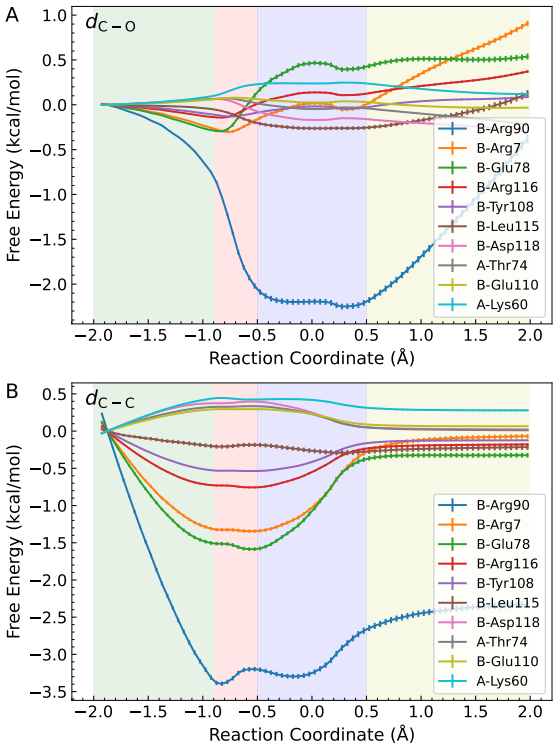

Figure 7: The free energy profiles of residue interaction from (A) the C–O bond breaking and (B) the C–C bond forming.

and through the C–O distance during stage II. Glu78 lowered the free energy barrier through the C–C distance shortening during stage I but increased the free energy barrier through C–O bond increase in stage II. In contrast, other key residues mainly contributed during stage I.

5 Conclusions

While QM/MM free energy simulations have become a valuable approach to studying enzymatic reactions, limited physical insights are gained by examining the resulting free energy profile alone. In this work, we presented an analysis tool that can decompose a free energy profile from QM/MM free energy simulations into physically meaningful components (such as different types of interactions, residue-by-residue contributions, and individual collective variable contributions) that can help us understand the functions of the enzyme and guide us to make rational decisions in designing enzymes.

However, precautions need to be taken when interpreting the results from this analysis for a number of reasons. First, like most decomposition schemes, the way the energy/force decomposition can be made is not unique. Second, the residue contributions to the total barrier should be considered as *in situ* contributions, i.e., the contribution of the residue with everything else fixed. It can deviate substantially from the actual barrier change with a residue removed or mutated, which will be accompanied by structural relaxations around the residue. The perturbed free energy profile due to a mutation of particular interest should be assessed by another QM/MM free energy simulation. Lastly, this work focuses entirely on the chemical step, where the bond breaking/formation takes place. For many enzyme complexes, a proposed mutation based on the 3D heatmap should also be subjected to binding free energy or conformational free energy simulations for a complete assessment of the mutation effect.

Acknowledgement The authors acknowledge the financial support from the National Institutes of Health: R01GM135392 (JP and YS), R44GM133270 (KN and YS), R01GM132481 and R01GM138472 (KN), and P30GM145423 (YS). YM acknowledges the support from San Diego State University Startup Fund. The authors thank the OU Supercomputing Center for Education & Research (OSCER) for the computational resources. YS also thanks Prof. Elfi Kraka for helpful suggestions.

Supporting Information Available

The following files are available free of charge.

- QM/MM interaction energy difference between the reactant and the transition state by residues for chorismate mutase (Table S1).

References

(1) Warshel, A. Electrostatic Origin of the Catalytic Power of Enzymes and the Role of Preorganized Active Sites. *J. Biol. Chem.* **1998**, *273*, 27035–27038.

(2) Garcia-Viloca, M.; Gao, J.; Karplus, M.; Truhlar, D. G. How Enzymes Work: Analysis by Modern Rate Theory and Computer Simulations. *Science* **2004**, *303*, 186–195.

(3) Li, W.-L.; Head-Gordon, T. Catalytic Principles from Natural Enzymes and Translational Design Strategies for Synthetic Catalysts. *ACS Cent. Sci.* **2021**, *7*, 72–80.

(4) Gao, J.; Xia, X. A Priori Evaluation of Aqueous Polarization Effects through Monte Carlo QM-MM Simulations. *Science* **1992**, *258*, 631–635.

(5) Boresch, S.; Archontis, G.; Karplus, M. Free Energy Simulations: The meaning of the Individual Contributions from a Component Analysis. *Proteins* **1994**, *20*, 25–33.

(6) Boresch, S.; Karplus, M. The Meaning of Component Analysis: Decomposition of the Free Energy in Terms of Specific Interactions. *J. Mol. Biol.* **1995**, *254*, 801–807.

(7) Gao, J. Energy Components of Aqueous Solution: Insight from Hybrid QM/MM Simulations Using a Polarizable Solvent Model. *J. Comput. Chem.* **1997**, *18*, 1061–1071.

(8) Bash, P. A.; Field, M. J.; Davenport, R. C.; Petsko, G. A.; Ringe, D.; Karplus, M. Computer simulation and analysis of the reaction pathway of triosephosphate isomerase. *Biochemistry* **1991**, *30*, 5826–5832.

(9) Karplus, M.; Evanseck, J. D.; Joseph, D.; Bash, P. A.; Field, M. J. Simulation Analysis of Triose Phosphate Isomerase: Conformational Transition and Catalysis. *Faraday Disc.* **1992**, *93*, 239.

(10) Cui, Q.; Karplus, M. Triosephosphate Isomerase: A Theoretical Comparison of Alternative Pathways. *J. Am. Chem. Soc.* **2001**, *123*, 2284–2290.

(11) Garcia-Viloca, M.; Truhlar, D. G.; Gao, J. Reaction-Path Energetics and Kinetics of the Hydride Transfer Reaction Catalyzed by Dihydrofolate Reductase. *Biochemistry* **2003**, *42*, 13558–13575.

(12) Ranaghan, K. E.; Ridder, L.; Szefczyk, B.; Sokalski, W. A.; Hermann, J. C.; Mulholland, A. J. Insights Into Enzyme Catalysis from QM/MM Modelling: Transition State Stabilization in Chorismate Mutase. *Mol. Phys.* **2003**, *101*, 2695–2714.

(13) Szefczyk, B.; Mulholland, A. J.; Ranaghan, K. E.; Sokalski, W. A. Differential Transition-State Stabilization in Enzyme Catalysis: Quantum Chemical Analysis of Interactions in the Chorismate Mutase Reaction and Prediction of the Optimal Catalytic Field. *J. Am. Chem. Soc.* **2004**, *126*, 16148–16159.

(14) Bhowmick, A.; Sharma, S. C.; Head-Gordon, T. The Importance of the Scaffold for *de Novo* Enzymes: A Case Study with Kemp Eliminase. *J. Am. Chem. Soc.* **2017**, *139*, 5793–5800.

(15) Vaissier, V.; Sharma, S. C.; Schaettle, K.; Zhang, T.; Head-Gordon, T. Computational Optimization of Electric Fields for Improving Catalysis of a Designed Kemp Eliminase. *ACS Catal.* **2018**, *8*, 219–227.

(16) Jaña, G. A.; Delgado, E. J.; Medina, F. E. How Important Is the Synclinal Conformation of Sulfonylureas To Explain the Inhibition of AHAS: A Theoretical Study. *J. Chem. Inf. Model.* **2014**, *54*, 926–932.

(17) Lee, F. S.; Chu, Z.-T.; Bolger, M. B.; Warshel, A. Calculations of Antibody-Antigen Interactions: Microscopic and Semimicroscopic Evaluation of the Free Energies of Binding of Phosphorylcholine Analogs to McPC603. *Protein Eng. Des. Sel.* **1992**, *5*, 215–228.

(18) Florián, J.; Goodman, M. F.; Warshel, A. Theoretical Investigation of the Binding Free Energies and Key Substrate-Recognition Components of the Replication Fidelity of Human DNA Polymerase β. *J. Phys. Chem. B* **2002**, *106*, 5739–5753.

(19) Klvaňa, M.; Jeřábek, P.; Goodman, M. F.; Florián, J. An Abridged Transition State Model To Derive Structure, Dynamics, and Energy Components of DNA Polymerase β Fidelity. *Biochemistry* **2011**, *50*, 7023–7032.

(20) Graham, S. E.; Syeda, F.; Cisneros, G. A. Computational Prediction of Residues Involved in Fidelity Checking for DNA Synthesis in DNA Polymerase I. *Biochemistry* **2012**, *51*, 2569–2578.

(21) Dewage, S. W.; Cisneros, G. A. Computational Analysis of Ammonia Transfer Along Two Intramolecular Tunnels in *Staphylococcus aureus* Glutamine-Dependent Amidotransferase (GatCAB). *J. Phys. Chem. B* **2015**, *119*, 3669–3677.

(22) Walker, A. R.; Cisneros, G. A. Computational Simulations of DNA Polymerases: Detailed Insights on Structure/Function/Mechanism from Native Proteins to Cancer Variants. *Chem. Res. Toxicol.* **2017**, *30*, 1922–1935.

(23) Maghsoud, Y.; Jayasinghe-Arachchige, V. M.; Kumari, P.; Cisneros, G. A.; Liu, J. Leveraging QM/MM and Molecular Dynamics Simulations to Decipher the Reaction Mechanism of the Cas9 HNH Domain to Investigate off-Target Effects. **2023**,

(24) Kędzierski, P.; Moskal, M.; Sokalski, W. A. Catalytic Fields as a Tool to Analyze Enzyme Reaction Mechanism Variants and Reaction Steps. *J. Phys. Chem. B* **2021**, *125*, 11606–11616.

(25) Hanoian, P.; Liu, C. T.; Hammes-Schiffer, S.; Benkovic, S. Perspectives on Electrostatics and Conformational Motions in Enzyme Catalysis. *Acc. Chem. Res.* **2015**, *48*, 482–489.

(26) Shaik, S.; Mandal, D.; Ramanan, R. Oriented Electric Fields as Future Smart Reagents in Chemistry. *Nature Chem.* **2016**, *8*, 1091–1098.

(27) Fried, S. D.; Boxer, S. G. Electric Fields and Enzyme Catalysis. *Annu. Rev. Biochem.* **2017**, *86*, 387–415.

(28) Shaik, S.; Ramanan, R.; Danovich, D.; Mandal, D. Structure and Reactivity/Selectivity Control by Oriented-External Electric Fields. *Chem. Soc. Rev.* **2018**, *47*, 5125–5145.

(29) Léonard, N. G.; Dhaoui, R.; Chantarojsiri, T.; Yang, J. Y. Electric Fields in Catalysis: From Enzymes to Molecular Catalysts. *ACS Catal.* **2021**, *11*, 10923–10932.

(30) Hennefarth, M. R.; Alexandrova, A. N. Advances in optimizing enzyme Electrostatic Preorganization. *Curr. Op. Struct. Biol.* **2022**, *72*, 1–8.

(31) Świderek, K.; Tuñón, I.; Moliner, V.; Bertran, J. Protein Flexibility and Preorganization in the Design of Enzymes. The Kemp Elimination Catalyzed by HG3.17. *ACS Catal.* **2015**, *5*, 2587–2595.

(32) Świderek, K.; Tuñón, I.; Williams, I. H.; Moliner, V. Insights on the Origin of Catalysis on Glycine *N* -Methyltransferase from Computational Modeling. *J. Am. Chem. Soc.* **2018**, *140*, 4327–4334.

(33) Galmés, M. A.; Nödling, A. R.; He, K.; Luk, L. Y. P.; Świderek, K.; Moliner, V. Computational Design of an Amidase by Combining the Best Electrostatic Features of Two Promiscuous Hydrolases. *Chem. Sci.* **2022**, *13*, 4779–4787.

(34) Fried, S. D.; Bagchi, S.; Boxer, S. G. Extreme electric fields power catalysis in the active site of ketosteroid isomerase. *Science* **2014**, *346*, 1510–1514.

(35) Wu, Y.; Boxer, S. G. A Critical Test of the Electrostatic Contribution to Catalysis with Noncanonical Amino Acids in Ketosteroid Isomerase. *J. Am. Chem. Soc.* **2016**, *138*, 11890–11895.

(36) Wu, Y.; Fried, S. D.; Boxer, S. G. A Preorganized Electric Field Leads to Minimal Geometrical Reorientation in the Catalytic Reaction of Ketosteroid Isomerase. *J. Am. Chem. Soc.* **2020**, *142*, 9993–9998.

(37) Hennefarth, M. R.; Alexandrova, A. N. Direct Look at the Electric Field in Ketosteroid Isomerase and Its Variants. *ACS Catal.* **2020**, *10*, 9915–9924.

(38) Zheng, C.; Mao, Y.; Kozuch, J.; Atsango, A. O.; Ji, Z.; Markland, T. E.; Boxer, S. G. A Two-Directional Vibrational Probe Reveals Different Electric Field Orientations in Solution and an Enzyme Active Site. *Nat. Chem.* **2022**, *14*, 891–897.

(39) Zheng, C.; Ji, Z.; Matthews, I. I.; Boxer, S. G. Enhanced active-site electric field accelerates enzyme catalysis. *Nat. Chem.* **2023**, 10.1038/s41557–023–01287–x.

(40) Liu, C. T.; Layfield, J. P.; Stewart, R. J.; French, J. B.; Hanoian, P.; Asbury, J. B.; Hammes-Schiffer, S.; Benkovic, S. J. Probing the Electrostatics of Active Site Microenvironments along the Catalytic Cycle for *Escherichia coli* Dihydrofolate Reductase. *J. Am. Chem. Soc.* **2014**, *136*, 10349–10360.
(41) Schyman, P.; Lai, W.; Chen, H.; Wang, Y.; Shaik, S. The Directive of the Protein: How Does Cytochrome P450 Select the Mechanism of Dopamine Formation? *J. Am. Chem. Soc.* **2011**, *133*, 7977–7984.
(42) Bím, D.; Alexandrova, A. N. Electrostatic Regulation of Blue Copper Sites. *Chem. Sci.* **2021**, *12*, 11406–11413.
(43) Xu, X.; Yan, S.; Hou, X.; Song, W.; Wang, L.; Wu, T.; Qi, M.; Wu, J.; Rao, Y.; Wang, B.; Liu, L. Local Electric Field Modulated Reactivity of *Pseudomonas aeruginosa* Acid Phosphatase for Enhancing Phosphorylation of l -Ascorbic Acid. *ACS Catal.* **2021**, *11*, 13397–13407.
(44) Peng, W.; Yan, S.; Zhang, X.; Liao, L.; Zhang, J.; Shaik, S.; Wang, B. How Do Preorganized Electric Fields Function in Catalytic Cycles? The Case of the Enzyme Tyrosine Hydroxylase. *J. Am. Chem. Soc.* **2022**, *144*, 20484–20494.
(45) Diao, W.; Yan, S.; Farrell, J. D.; Wang, B.; Ye, F.; Wang, Z. Preorganized Internal Electric Field Powers Catalysis in the Active Site of Uracil-DNA Glycosylase. *ACS Catal.* **2022**, *12*, 12488–12499.
(46) Fried, S. D.; Bagchi, S.; Boxer, S. G. Measuring electrostatic fields in both hydrogen-bonding and non-hydrogen-bonding environments using carbonyl vibrational probes. *J. Am. Chem. Soc.* **2013**, *135*, 11181–11192.
(47) Krzemińska, A.; Moliner, V.; Świderek, K. Dynamic and Electrostatic Effects on the Reaction Catalyzed by HIV-1 Protease. *J. Am. Chem. Soc.* **2016**, *138*, 16283–16298.
(48) Galmés, M. A.; Nödling, A. R.; Luk, L.; Świderek, K.; Moliner, V. Combined Theoretical and Experimental Study to Unravel the Differences in Promiscuous Amidase Activity of Two Nonhomologous Enzymes. *ACS Catal.* **2021**, *11*, 8635–8644.
(49) Torrie, G. M.; Valleau, J. P. Monte Carlo Free Energy Estimates Using Non-Boltzmann Sampling: Application to the Sub-Critical Lennard-Jones Fluid. *Chem. Phys. Lett.* **1974**, *28*, 578–581.
(50) Kästner, J.; Thiel, W. Bridging the gap between thermodynamic integration and umbrella sampling provides a novel analysis method: "Umbrella integration". *J. Chem. Phys.* **2005**, *123*, 144104.
(51) den Otter, W. K. Thermodynamic integration of the free energy along a reaction coordinate in Cartesian coordinates. *J. Chem. Phys.* **2000**, *112*, 7283–7292.
(52) Hénin, J.; Fiorin, G.; Chipot, C.; Klein, M. L. Exploring Multidimensional Free Energy Landscapes Using Time-Dependent Biases on Collective Variables. *J. Chem. Theory Comput.* **2009**, *6*, 35–47.
(53) Fiorin, G.; Klein, M. L.; Hénin, J. Using collective variables to drive molecular dynamics simulations. *Mol. Phys.* **2013**, *111*, 3345–3362.
(54) Comer, J.; Gumbart, J. C.; Hénin, J.; Lelièvre, T.; Pohorille, A.; Chipot, C. The Adaptive Biasing Force Method: Everything You Always Wanted To Know but Were Afraid To Ask. *J. Phys. Chem. B* **2014**, *119*, 1129–1151.
(55) Roux, B.; Karplus, M. Ion transport in a model gramicidin channel. Structure and thermodynamics. *Biophysical Journal* **1991**, *59*, 961–981.
(56) Dorairaj, S.; Allen, T. W. On the thermodynamic stability of a charged arginine side chain in a transmembrane helix. *Proc. Natl. Acad. Sci.* **2007**, *104*, 4943–4948.
(57) Cerutti, D. S.; Rice, J. E.; Swope, W. C.; Case, D. A. Derivation of Fixed Partial Charges for Amino Acids Accommodating a Specific Water Model and Implicit Polarization. *J. Phys. Chem. B* **2013**, *117*, 2328–2338.
(58) Sodt, A. J.; Mei, Y.; Koenig, G.; Tao, P.; Steele, R. P.; Brooks, B. R.; Shao, Y. Multiple Environment Single System Quantum Mechanical/Molecular Mechanical (MESS-QM/MM) Calculations. 1. Estimation of Polarization Energies. *J. Phys. Chem. A* **2015**, *119*, 1511–1523.
(59) Pan, X.; Yang, J.; Van, R.; Epifanovsky, E.; Ho, J.; Huang, J.; Pu, J.; Mei, Y.; Nam, K.; Shao, Y. Machine-Learning-Assisted Free Energy Simulation of Solution-Phase and Enzyme Reactions. *J. Chem. Theory Comput.* **2021**, *17*, 5745–5758.
(60) Chook, Y. M.; Ke, H.; Lipscomb, W. N. Crystal Structures of the Monofunctional Chorismate Mutase from Bacillus Subtilis and Its Complex with a Transition State Analog. *Proc. Natl. Acad. Sci.* **1993**, *90*, 8600–8603.
(61) Jorgensen, W. L.; Chandrasekhar, J.; Madura, J. D.; Impey, R. W.; Klein, M. L. Comparison of Simple Potential Functions for Simulating Liquid Water. *J. Chem. Phys.* **1983**, *79*, 926–935.
(62) Wang, J.; Wolf, R. M.; Caldwell, J. W.; Kollman, P. A.; Case, D. A. Development and Testing of a General Amber Force Field. *J. Comput. Chem.* **2004**, *25*, 1157–1174.
(63) Maier, J. A.; Martinez, C.; Kasavajhala, K.; Wickstrom, L.; Hauser, K. E.; Simmerling, C. ff14SB: Improving the Accuracy of Protein Side Chain and Backbone Parameters from ff99SB. *J. Chem. Theory Comput.* **2015**, *11*, 3696–3713.
(64) Becke, A. D. Density-Functional Exchange-Energy Approximation with Correct Asymptotic Behavior. *Phys. Rev. A* **1988**, *38*, 3098–3100.
(65) Becke, A. D. A New Mixing of Hartree–Fock and Local Density-Functional Theories. *J. Chem. Phys.* **1993**, *98*, 1372–1377.
(66) Lee, C.; Yang, W.; Parr, R. G. Development of the Colle-Salvetti Correlation-Energy Formula into a Functional of the Electron Density. *Phys. Rev. B* **1988**, *37*, 785–789.
(67) Hariharan, P. C.; Pople, J. A. The Influence of Polarization Functions on Molecular Orbital Hydrogenation Energies. *Theor. Chim. Acta* **1973**, *28*, 213–222.
(68) Darden, T.; York, D.; Pedersen, L. Particle Mesh Ewald: AnN·log(N) Method for Ewald Sums in Large Systems. *J. Chem. Phys.* **1993**, *98*, 10089–10092.
(69) Essmann, U.; Perera, L.; Berkowitz, M. L.; Darden, T.; Lee, H.; Pedersen, L. G. A Smooth Particle Mesh Ewald Method. *J. Chem. Phys.* **1995**, *103*, 8577–8593.
(70) Pan, X.; Nam, K.; Epifanovsky, E.; Simmonett, A. C.; Rosta, E.; Shao, Y. A Simplified Charge Projection Scheme for Long-Range Electrostatics in ab initio QM/MM Calculations. *J. Chem. Phys.* **2021**, *154*, 024115.
(71) Ryckaert, J.-P.; Ciccotti, G.; Berendsen, H. J. Numerical Integration of the Cartesian Equations of Motion of a System with Constraints: Molecular Dynamics of n-Alkanes. *J. Comput. Phys.* **1977**, *23*, 327–341.
(72) Case, D. A.; Belfon, K.; Ben-Shalom, I. Y.; Brozell, S. R.; Cerutti, D. S.; Cheatham, T. E.; III,; Cruzeiro, V. W. D.; Darden, T. A.; Duke, R. E.; Giambasu, G.; Gilson, M. K.; Gohlke, H.; Goetz, A. W.; Harris, R.; Izadi, S.; Izmailov, S. A.; Kasavajhala, K.; Kovalenko, A.; Krasny, R.; Kurtzman, T.; Lee, T. S.; LeGrand, S.; Li, P.; Lin, C.; Liu, J.; Luchko, T.; Luo, R.; Man, V.; Merz, K. M.; Miao, Y.; Mikhailovskii, O.; Monard, G.; Nguyen, H.; Onufriev, A.; Pan, F.; Pantano, S.; Qi, R.; Roe, D. R.; Roitberg, A.; Sagui, C.; Schott-Verdugo, S.;

Shen, J.; Simmerling, C.; Skrynnikov, N. R.; Smith, J.; Swails, J.; Walker, R. C.; Wang, J.; Wilson, L.; Wolf, R. M.; Wu, X.; Xiong, Y.; Xue, Y.; York, D. M.; Kollman, P. A. AMBER 2020, University of California, San Francisco. 2020.

(73) Epifanovsky, E.; Gilbert, A. T. B.; Feng, X.; Lee, J.; Mao, Y.; Mardirossian, N.; Pokhilko, P.; White, A. F.; Coons, M. P.; Dempwolff, A. L.; Gan, Z.; Hait, D.; Horn, P. R.; Jacobson, L. D.; Kaliman, I.; Kussmann, J.; Lange, A. W.; Lao, K. U.; Levine, D. S.; Liu, J.; McKenzie, S. C.; Morrison, A. F.; Nanda, K. D.; Plasser, F.; Rehn, D. R.; Vidal, M. L.; You, Z.-Q.; Zhu, Y.; Alam, B.; Albrecht, B. J.; Aldossary, A.; Alguire, E.; Andersen, J. H.; Athavale, V.; Barton, D.; Begam, K.; Behn, A.; Bellonzi, N.; Bernard, Y. A.; Berquist, E. J.; Burton, H. G. A.; Carreras, A.; Carter-Fenk, K.; Chakraborty, R.; Chien, A. D.; Closser, K. D.; Cofer-Shabica, V.; Dasgupta, S.; de Wergifosse, M.; Deng, J.; Diedenhofen, M.; Do, H.; Ehlert, S.; Fang, P.-T.; Fatehi, S.; Feng, Q.; Friedhoff, T.; Gayvert, J.; Ge, Q.; Gidofalvi, G.; Goldey, M.; Gomes, J.; González-Espinoza, C. E.; Gulania, S.; Gunina, A. O.; Hanson-Heine, M. W. D.; Harbach, P. H. P.; Hauser, A.; Herbst, M. F.; Hernández Vera, M.; Hodecker, M.; Holden, Z. C.; Houck, S.; Huang, X.; Hui, K.; Huynh, B. C.; Ivanov, M.; Jász, A.; Ji, H.; Jiang, H.; Kaduk, B.; Kähler, S.; Khistyaev, K.; Kim, J.; Kis, G.; Klunzinger, P.; Koczor-Benda, Z.; Koh, J. H.; Kosenkov, D.; Koulias, L.; Kowalczyk, T.; Krauter, C. M.; Kue, K.; Kunitsa, A.; Kus, T.; Ladjánszki, I.; Landau, A.; Lawler, K. V.; Lefrancois, D.; Lehtola, S.; Li, R. R.; Li, Y.-P.; Liang, J.; Liebenthal, M.; Lin, H.-H.; Lin, Y.-S.; Liu, F.; Liu, K.-Y.; Loipersberger, M.; Luenser, A.; Manjanath, A.; Manohar, P.; Mansoor, E.; Manzer, S. F.; Mao, S.-P.; Marenich, A. V.; Markovich, T.; Mason, S.; Maurer, S. A.; McLaughlin, P. F.; Menger, M. F. S. J.; Mewes, J.-M.; Mewes, S. A.; Morgante, P.; Mullinax, J. W.; Oosterbaan, K. J.; Paran, G.; Paul, A. C.; Paul, S. K.; Pavošević, F.; Pei, Z.; Prager, S.; Proynov, E. I.; Rák, A.; Ramos-Cordoba, E.; Rana, B.; Rask, A. E.; Rettig, A.; Richard, R. M.; Rob, F.; Rossomme, E.; Scheele, T.; Scheurer, M.; Schneider, M.; Sergueev, N.; Sharada, S. M.; Skomorowski, W.; Small, D. W.; Stein, C. J.; Su, Y.-C.; Sundstrom, E. J.; Tao, Z.; Thirman, J.; Tornai, G. J.; Tsuchimochi, T.; Tubman, N. M.; Veccham, S. P.; Vydrov, O.; Wenzel, J.; Witte, J.; Yamada, A.; Yao, K.; Yeganeh, S.; Yost, S. R.; Zech, A.; Zhang, I. Y.; Zhang, X.; Zhang, Y.; Zuev, D.; Aspuru-Guzik, A.; Bell, A. T.; Besley, N. A.; Bravaya, K. B.; Brooks, B. R.; Casanova, D.; Chai, J.-D.; Coriani, S.; Cramer, C. J.; Cserey, G.; DePrince, A. E.; DiStasio, R. A.; Dreuw, A.; Dunietz, B. D.; Furlani, T. R.; Goddard, W. A.; Hammes-Schiffer, S.; Head-Gordon, T.; Hehre, W. J.; Hsu, C.-P.; Jagau, T.-C.; Jung, Y.; Klamt, A.; Kong, J.; Lambrecht, D. S.; Liang, W.; Mayhall, N. J.; McCurdy, C. W.; Neaton, J. B.; Ochsenfeld, C.; Parkhill, J. A.; Peverati, R.; Rassolov, V. A.; Shao, Y.; Slipchenko, L. V.; Stauch, T.; Steele, R. P.; Subotnik, J. E.; Thom, A. J. W.; Tkatchenko, A.; Truhlar, D. G.; Van Voorhis, T.; Wesolowski, T. A.; Whaley, K. B.; Woodcock, H. L.; Zimmerman, P. M.; Faraji, S.; Gill, P. M. W.; Head-Gordon, M.; Herbert, J. M.; Krylov, A. I. Software for the frontiers of quantum chemistry: An overview of developments in the Q-Chem 5 package. *J. Chem. Phys.* **2021**, *155*, 084801.

(74) Fukunishi, H.; Watanabe, O.; Takada, S. On the Hamiltonian Replica Exchange Method for Efficient Sampling of Biomolecular Systems: Application to Protein Structure Prediction. *J. Chem. Phys.* **2002**, *116*, 9058–9067.

(75) Shirts, M. R.; Chodera, J. D. Statistically Optimal Analysis of Samples from Multiple Equilibrium States. *J. Chem. Phys.* **2008**, *129*, 124105.

(76) Sugita, Y.; Kitao, A.; Okamoto, Y. Multidimensional replica-exchange method for free-energy calculations. *J. Chem. Phys.* **2000**, *113*, 6042–6051.

(77) Kuechler, E. R.; Giese, T. J.; York, D. M. Charge-Dependent Many-Body Exchange and Dispersion Interactions in Combined QM/MM Simulations. *J. Chem. Phys.* **2015**, *143*, 234111.

(78) Giovannini, T.; Lafiosca, P.; Cappelli, C. A General Route to Include Pauli Repulsion and Quantum Dispersion Effects in QM/MM Approaches. *J. Chem. Theory Comput.* **2017**, *13*, 4854–4870.

(79) Slipchenko, L. V.; Gordon, M. S.; Ruedenberg, K. Dispersion Interactions in QM/EFP. *J. Phys. Chem. A* **2017**, *121*, 9495–9507.

(80) Viquez Rojas, C. I.; Fine, J.; Slipchenko, L. V. Exchange-Repulsion Energy in QM/EFP. *J. Chem. Phys.* **2018**, *149*, 094103.

(81) Cload, S. T.; Liu, D. R.; Pastor, R. M.; Schultz, P. G. Mutagenesis Study of Active Site Residues in Chorismate Mutase from *Bacillus subtilis*. *J. Am. Chem. Soc.* **1996**, *118*, 1787–1788.

(82) Kienhöfer, A.; Kast, P.; Hilvert, D. Selective Stabilization of the Chorismate Mutase Transition State by a Positively Charged Hydrogen Bond Donor. *J. Am. Chem. Soc.* **2003**, *125*, 3206–3207.

(83) Lyne, P. D.; Mulholland, A. J.; Richards, W. G. Insights into Chorismate Mutase Catalysis from a Combined QM/MM Simulation of the Enzyme Reaction. *J. Am. Chem. Soc.* **1995**, *117*, 11345–11350.

(84) Worthington, S. E.; Roitberg, A. E.; Krauss, M. An MD/QM Study of the Chorismate Mutase-Catalyzed Claisen Rearrangement Reaction. *J. Phys. Chem. B* **2001**, *105*, 7087–7095.

(85) Ishida, T.; Fedorov, D. G.; Kitaura, K. All Electron Quantum Chemical Calculation of the Entire Enzyme System Confirms a Collective Catalytic Device in the Chorismate Mutase Reaction. *J. Phys. Chem. B* **2005**, *110*, 1457–1463.

(86) Szefczyk, B.; Claeyssens, F.; Mulholland, A. J.; Sokalski, W. A. Quantum chemical analysis of reaction paths in chorismate mutase: Conformational effects and electrostatic stabilization. *Int. J. Quantum Chem.* **2007**, *107*, 2274–2285.

(87) Ishida, T. Probing protein environment in an enzymatic process: All-electron quantum chemical analysis combined with *ab initio* quantum mechanical/molecular mechanical modeling of chorismate mutase. *J. Chem. Phys.* **2008**, *129*, 125105.

TOC Graphic